

LQG controller designs from reduced order models for a launch vehicle

ASHWIN DHABALE, R N BANAVAR[†] and M V DHEKANE[‡]

[†]Systems and Control Engineering, Indian Institute of Technology Bombay, Mumbai 400 076

[‡]Control and Guidance Group, Vikram Sarabhai Space Centre, Indian Space Research Organization, Thiruvananthapuram 695 022
e-mail: banavar@iitb.ac.in

MS received 6 April 2006; revised 28 August 2007

Abstract. The suppression of liquid fuel slosh motion is critical in a launch vehicle (LV). In particular, during certain stages of the launch, the dynamics of the fuel interacts adversely with the rigid body dynamics of the LV and the feedback controller must attenuate these effects. This paper describes the effort of a multi-variable control approach applied to the Geosynchronous Satellite Launch Vehicle (GSLV) of the Indian Space Research Organization (ISRO) during a certain stage of its launch. The fuel slosh dynamics are modelled using a pendulum model analogy. We describe two design methodologies using the Linear-Quadratic Gaussian (LQG) technique. The novelty of the technique is that we apply the LQG design for models that are reduced in order through inspection alone. This is possible from a perspective that the LV could be viewed as many small systems attached to a main body and the interactions of some of these smaller systems could be neglected at the controller design stage provided sufficient robustness is ensured by the controller. The first LQG design is carried out without the actuator dynamics incorporated at the design stage and for the second design we neglect the slosh dynamics as well.

Keywords. Launch vehicle; fuel slosh; LQG controller design.

1. Introduction

The wave motion of liquids in finite containers, commonly known as slosh, is known to have adverse effects on aerospace vehicles Abramson (1966), Dodge & Garza (1967). For example, propellant slosh in rockets can have a detrimental effect during lift off, while fuel slosh in aircrafts and spacecrafts can effect control system performance during vehicle manoeuvres. To mitigate these effects a variety of techniques have been proposed including the use of baffles and dampers. These techniques are inherently passive in nature since energy dissipation is primary goal. To go beyond passive slosh suppression, several researches have investigated the feasibility of applying active feedback control (Reyhanoglu *et al* 1999, 2000).

In this paper, the control of a LV with significant fuel slosh dynamics is considered. The objective is to simultaneously control the rigid body motion while suppressing the sloshing of

the fuel, using only the control effectors (strap-ons) that act on the rigid vehicle. Suppression of the unactuated fuel slosh degree of freedom must be achieved through the system coupling. Here, the fuel slosh dynamics are modelled using a pendulum model analogy. These pendulums have no actuation and it is critical to keep their oscillations small. Four actuators (each consisting of an engine and a nozzle) are symmetrically attached to the periphery of the central cylindrical core. The actuators are modelled as one-dimensional pendulums since the nozzles are hinged such that they can move in only one plane. The control inputs are defined by the four actuator deflection angles. The entire LV model is numerically badly conditioned, uncontrollable, unobservable and unstable as well.

A preliminary version of this paper was presented at the International Federation of Automatic Control (IFAC) World Congress 2005 (Dhabale *et al* 2005). The paper is organized as follows. The model of the LV with the actuator and fuel slosh dynamics has been developed by ISRO in the form of linear differential equations in the descriptor form. The model is a perturbation model about a nominal operating condition. In § 3 we describe the various components that build up the model of the launch vehicle. In § 4 we develop a state-space model of the system from the set of descriptor equations. This state-space model is useful for the LQ controller design. Section 5 of the paper applies LQG synthesis technique to suppress the effects of the fuel slosh aroused due to application of input with a strap-on nozzle as an actuator. Simulation results that demonstrate the closed-loop performance are presented in § 6. Conclusions are drawn in § 7.

2. Model formulation

We utilize a mathematical model that describes the accelerating flight of a launch vehicle (LV) in a fixed plane. The pitch-roll dynamics is considered here and the same results are applicable to the yaw-roll channel as well since the LV is symmetrical about the vertical axis. The LV dynamic model used is provided by Vikram Sarabhai Space Centre of ISRO. The equations derived are similar to those presented for a LV in (Greensite 1972). This model describes linear perturbation dynamics for the pitch plane and includes lateral motion, pitching, rolling, first sloshing mode and second order actuator dynamics. The schematic of the LV is shown in figure 1. Four strap-ons are symmetrically attached on the periphery of the central core. The control input is the nozzle deflection angle. Strap-ons 2 and 4 control the pitching of the LV and all four are responsible for rolling. The sign convention for the deflection of the 2nd and 4th strap-on is chosen according to the pitching requirement. Hence for the 4th strap-on, a positive deflection in the sense of pitching causes roll in the negative direction. This is seen in equation (11) where a negative sign manifests for the 4th strap-on control. The variables of interest are the attitude angle θ of the vehicle with respect to a fixed inertial reference, the rolling angle ϕ of the vehicle, the actuator deflection angles δ_i and slosh pendulum angles τ_{pi} with respect to vehicle longitudinal axis. The pitching and rolling motions are produced by the component $T_c \sin \delta_i$ of the thrust. The mass and moment of inertia of the vehicle and engine are constant in the problem. We now briefly describe the sub-component dynamics.

2.1 Sub-component dynamics

As shown in the figure 1 the LV is symmetrical about its longitudinal axis. Hence the equations developed in pitch plane are applicable in the yaw plane with appropriate modifications. Here, all the forces and moments are calculated in the pitch ($x - z$) plane. The component of forces along the vehicle longitudinal axis only accelerate the vehicle and hence are not of interest for control.

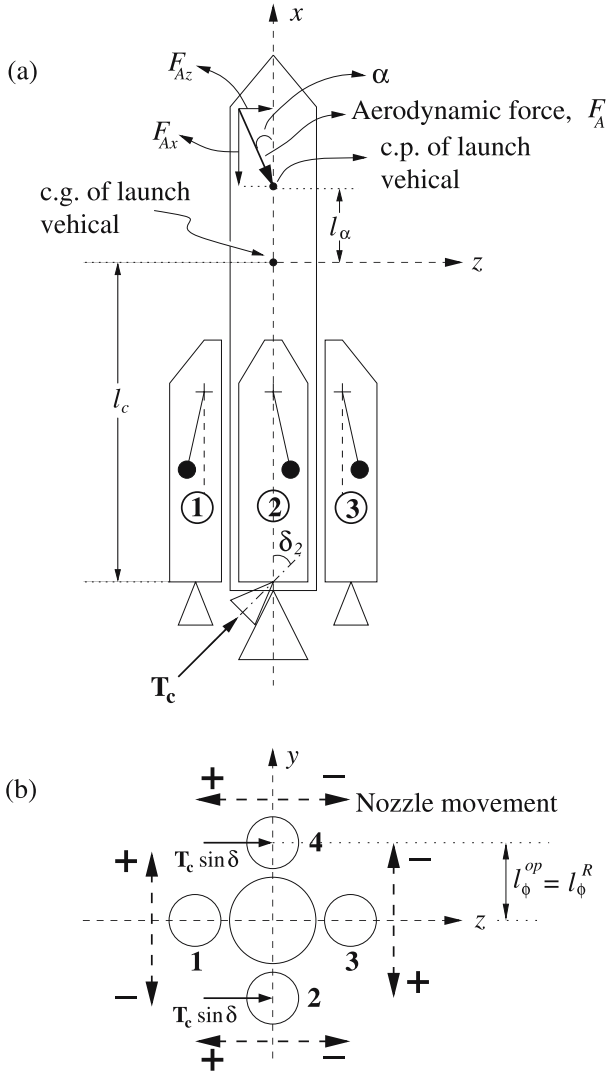


Figure 1. (a): Schematic of the rocket front view, (b): Schematic of the rocket top view.

2.1a *Thrust:* Refer to figure 1(a),

$$F_{zT} = T_c \sin \delta_2 \approx T_c \delta_2; \quad \sin \delta_2 \text{ is small}$$

$$M_{yT} = l_c T_c \delta_2. \tag{1}$$

These expressions are the same for all the nozzles.

2.1b *Sloshing:* Consider the schematic of the slosh pendulum shown in figure 2. The velocity of this pendulum relative to inertial space is given by

$$\mu_{pi} = \mu + \frac{\partial \rho_{pi}}{\partial t} + \omega \times \rho_{pi}, \tag{2}$$

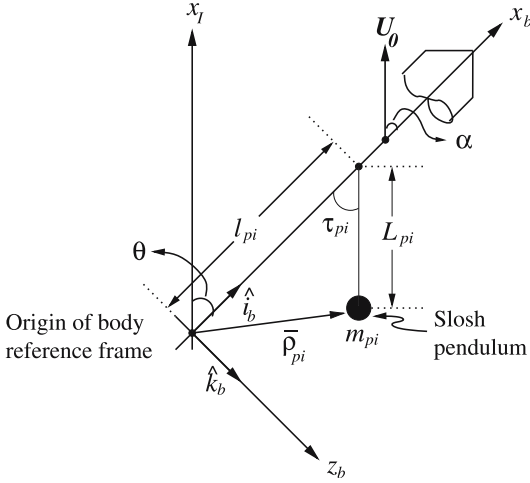


Figure 2. Schematic of a slosh pendulum.

where μ is velocity of vehicle c.g. with respect to inertial reference and ω is the angular velocity about the inertial reference y -axis. The kinetic energy is

$$K = \frac{1}{2} m_{pi} \mu_{pi}^T \mu_{pi}.$$

There is no potential energy since the system is in free fall. The Lagrangian is $L = K$ and the Euler–Lagrange equations are

$$\frac{d}{dt} \left(\frac{\partial L}{\partial \dot{\tau}_{pi}} \right) - \frac{\partial L}{\partial \tau_{pi}} = 0.$$

Performing the indicated operations, assuming τ_{pi} and $\dot{\tau}_{pi}$ are small quantities and noting that $\dot{Q} = 0$, gives

$$\ddot{\tau}_{pi} + \omega_{pi}^2 \tau_{pi} = \frac{1}{L_{pi}} [U_0 \dot{\theta} - \dot{w} + \ddot{\theta} (l_{pi} - L_{pi})], \quad (3)$$

U_0 is the steady state value of the vehicle velocity along the inertial x -axis, and \dot{w} is vehicle acceleration in the inertial z -direction. Equation (3) is the equation of motion of the i^{th} pendulum in the pitch plane. The sloshing forces and moments now appear as

$$F_{zs} = \sum_i m_{pi} \dot{U}_0 \tau_{pi}$$

$$M_{ys} = \sum_i m_{pi} l_{pi} \dot{U}_0 \tau_{pi}. \quad (4)$$

2.1c Engine inertia: There are two kinds of forces exerted by the engine on the launch vehicle. One is the reaction of the rotation of the engine and the second is due to the external torque applied to the engine, alike the force exerted by slosh pendulums. The engine and the

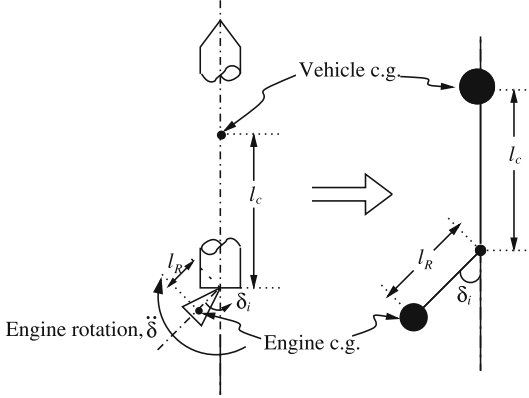


Figure 3. Engine parameters for single strap-on.

launch vehicle are treated as two pendulums connected to each other in the free space, as shown in figure 3. The force exerted by the engine on the vehicle is

$$F_{zE} = m_R l_R \ddot{\delta}_i. \quad (5)$$

An external torque applied to the engine is represented by

$$M_{yE}^{(1)} = m_R l_R \dot{U}_0 \delta_i. \quad (6)$$

The result is that a total torque of magnitude, $(M_{yE}^{(1)} + F_{zE} l_c)$, is applied to the vehicle in the positive θ direction due to engine inertia forces

$$M_{yE} = (I_R + m_R l_R l_c) \ddot{\delta}_i + m_R l_R \dot{U}_0 \delta_i. \quad (7)$$

2.1d Aerodynamic forces: The aerodynamic force acts at the center of pressure of the LV. It acts along the line of the vehicle velocity, that is making an angle equal to the angle of attack with the axis of the launch vehicle as shown in figure 1 and can be described as

$$F_{Az} = C_z s q$$

and

$$F_{Ax} = C_x s q,$$

where C_z and C_x are non-dimensional normal and chord force coefficients, respectively, and are primarily functions of vehicle shape. The term s is a convenient reference area (usually the maximum body cross-section), and q is the dynamic pressure ($= \frac{1}{2} \rho v^2$, where ρ is air density, and v is velocity) [?]. Further,

$$C_z = \left[\frac{\partial C_z}{\partial \alpha} \right] \alpha = C_{z\alpha} \alpha.$$

Hence if $C_{z\alpha}$, s and q are constants, the aerodynamic force becomes

$$F_{Az} = L_\alpha \alpha \quad \text{where,} \quad L_\alpha = C_{z\alpha} s q. \quad (8)$$

2.2 Short period dynamics equations for pitch/roll coupled system

The forces and moments given in the previous sub-section are now incorporated to give the final linearized short period model frozen at an instant and valid for short time. So we have the following equations.

2.2a *Pitching*: All the moments acting about vehicle body y-axis are summed to yield

$$I_{yy}\ddot{\theta} = \sum_{i=2,4} (I_R + m_R l_R l_c) \ddot{\delta}_i + [L_\alpha l_\alpha] \alpha - \sum_{i=1}^8 [\dot{U}_0 m_{pi} l_{pi}] \tau_{pi} + \sum_{i=2,4} (T_c l_c + m_R l_R \dot{U}_0) \delta_i. \quad (9)$$

Each strap-on has two compartments one for fuel and the other for oxidizer hence there are total of eight pendulums.

2.2b *Lateral motion*: All the forces producing the acceleration in the vehicle body z-direction are summarized to give

$$(m_0 U_0)(\dot{\alpha} - \dot{\theta}) = \sum_{i=2,4} [m_R l_R] \ddot{\delta}_i - [L_\alpha] \alpha + \sum_{i=1}^8 [m_{pi} \dot{U}_0] \tau_{pi} + \sum_{i=2,4} [T_c] \delta_i. \quad (10)$$

2.2c *Rolling*: All the moments in the roll direction give

$$I_{xx}\ddot{\phi} = \sum_{i=1}^3 [T_c l_{\phi_i}^R + m_R \dot{U}_0 l_{\phi_i}^R] \delta_i + \sum_{i=1}^3 [m_R l_R l_{\phi_i}^R] \ddot{\delta}_i - [T_c l_{\phi_4}^R + m_R \dot{U}_0 l_{\phi_4}^R] \delta_4 - [m_R l_R l_{\phi_4}^R] \ddot{\delta}_4 + \sum_{i=1}^8 [m_{pi} \dot{U}_0 l_{\phi_i}^{op}] \tau_i. \quad (11)$$

2.2d *Slosh*: Slosh pendulums have second order dynamics given by

$$\ddot{\tau}_{pi} + 2\zeta_{pi}\omega_{pi}\dot{\tau}_{pi} + \omega_{pi}^2\tau_{pi} = [(l_{pi} - L_{pi})/L_{pi}]\ddot{\theta} - [U_0/L_{pi}]\dot{\alpha} - [l_{\phi_i}/L_{pi}]\ddot{\phi} + [U_0/L_{pi}]\dot{\theta}, \quad (12)$$

where the terms on the right hand side are forcing functions on the pendulums.

2.2e *Actuator dynamics*: As shown in figure 3, the nozzle is considered as a pendulum and is modelled as

$$\ddot{\delta}_i = \omega_a^2 \delta_c - 2\zeta_a \omega_a \dot{\delta}_i - \omega_a^2 \delta_i, \quad (13)$$

where ω_a is the natural frequency, ζ_a the damping coefficient and $\omega_a^2 \delta_c$ is the forcing function, where δ_c is the desired nozzle deflection. The autopilot command δ_P for the pitch loop and

δ_R for roll are transformed into four actuator commands as given in the transformation matrix T as follows:

$$\underbrace{\begin{bmatrix} \delta_{1c} \\ \delta_{2c} \\ \delta_{3c} \\ \delta_{4c} \end{bmatrix}}_{\mathbf{u}} = \underbrace{\begin{bmatrix} 0 & 1 \\ 1 & 1 \\ 0 & 1 \\ 1 & -1 \end{bmatrix}}_{\mathbf{T}} * \underbrace{\begin{bmatrix} \delta_P \\ \delta_R \end{bmatrix}}_{\mathbf{u}'} \quad (14)$$

2.2f *Sensors:* The sensors are rate and angle gyros modelled as second order systems given by the following transfer functions.

Sensors for angles

$$G_P = \frac{\omega_1^2}{s^2 + 2\xi_1\omega_1s + \omega_1^2}, \text{ where } \omega_1 = 17.5 \text{ Hz} = 109.96 \text{ rad/sec and } \xi_1 = 0.7.$$

Sensors in Rate path

$$G_R = \frac{\omega_2^2}{s^2 + 2\xi_2\omega_2s + \omega_2^2}, \text{ where } \omega_2 = 12.5 \text{ Hz} = 78.54 \text{ rad/sec and } \xi_2 = 0.7.$$

3. Formulation of the state space model

The vehicle dynamics including rigid body, slosh and actuators can be written in a descriptor state space form as

$$\begin{aligned} K\dot{x} &= Ax + Bu \\ y &= Cx + Du \end{aligned} \quad (15)$$

where,

$$\begin{aligned} x &\in \mathbb{R}^{29} : \text{ the vehicle state vector,} \\ u &\in \mathbb{R}^4 : \text{ pitch and roll control signal, defined in (14),} \\ y &\in \mathbb{R}^4 : \text{ output vector, } y = [\theta, \dot{\theta}, \phi, \dot{\phi}]^T, \end{aligned}$$

and A, K, B, C, D have appropriate dimensions.

The 29 state variables are $\theta, \dot{\theta}, \alpha, \phi, \dot{\phi}, \tau_i, \dot{\tau}_i \dots i = 1$ to 8 and, $\delta_j, \dot{\delta}_j \dots j = 1$ to 4. The matrix K is invertible, hence the system can be transformed into a standard state space form

$$\dot{x} = A_1x + B_1u, \quad (16)$$

where $A_1 = K^{-1}A$ and $B_1 = K^{-1}B$. The system (16) is a 4 input and 4 output system. The inputs to the system are the desired actuator deflections but the signal generated by the controller are the pitch and roll angles. Hence by substituting (14) in (16) the system is now re-written as a 2 input 4 output system as

$$\dot{x} = A_1x + B'_1u', \quad (17)$$

where, $B'_1 = B_1 \mathbf{T}$. The system (17) is analysed and found to be unstable, uncontrollable and unobservable. This makes the system unsuitable for LQG controller design. To circumvent these problems, we carry out some conditioning and model order reduction on the system.

Standard model order reduction techniques are not applicable here due to the unstable nature of the system. The model order is reduced by inspecting the system equations. We return to the system in the form given by (15) for this purpose. It is observed that with some assumptions on the magnitudes of the coefficients in the K matrix, we are able to separate the actuator dynamics as follows.

$$\underbrace{\begin{bmatrix} K_{21 \times 21} & K_{21 \times 8} \approx 0 \\ \mathcal{O}_{8 \times 21} & K_{\text{act}} = I_{8 \times 8} \end{bmatrix}}_{K_{29 \times 29}} \begin{bmatrix} \dot{x}_0 \\ \dot{\Delta} \end{bmatrix} = \underbrace{\begin{bmatrix} A_{21 \times 21} & K_{21 \times 8}^* \\ \mathcal{O}_{8 \times 21} & A_{\text{act}} \end{bmatrix}}_{A_{29 \times 29}} \begin{bmatrix} x_0 \\ \Delta \end{bmatrix} + \begin{bmatrix} B_{21 \times 4} = 0 \\ B_{8 \times 4} \end{bmatrix} u$$

which we write as

$$\underbrace{\begin{bmatrix} K_{11} & K_{12} \\ K_{21} & K_{22} \end{bmatrix}}_{K_{29 \times 29}} \begin{bmatrix} \dot{x}_0 \\ \dot{\Delta} \end{bmatrix} = \underbrace{\begin{bmatrix} A_{11} & K_{12} \\ A_{21} & A_{22} \end{bmatrix}}_{A_{29 \times 29}} \begin{bmatrix} x_0 \\ \Delta \end{bmatrix} + \begin{bmatrix} B_{11} \\ B_{21} \end{bmatrix} u$$

$$\Rightarrow \left. \begin{array}{l} \dot{\Delta} = A_{\text{act}} \Delta + B_{8 \times 4} u \\ y_{\text{act}} = C_{\text{act}} \Delta \end{array} \right\| \begin{array}{l} \text{Actuator} \\ \text{Launchvehicle} \\ \hline K_{21 \times 21} \dot{x}_0 = A_{21 \times 21} x_0 + B_{21 \times 4}^* y_{\text{act}} \\ y = C_0 x_0 \end{array}$$

where, $K_{11} \in \mathbb{R}^{21 \times 21}$, $K_{12} \in \mathbb{R}^{21 \times 8}$ contains entries which are small and is approximated to zero, $K_{21} = [0]_{8 \times 21}$ and $K_{22} = [I]_8$. Also $A_{21} = [0]_{8 \times 21}$. $B_{11} \in \mathbb{R}^{21 \times 4}$ and $B_{21} \in \mathbb{R}^{8 \times 4}$.

The left hand side set of equations describe an 8th-order actuator system

$$\begin{aligned} \dot{\Delta} &= A_{\text{act}} \Delta + B_{\text{act}} u' \\ y_{\text{act}} &= C_{\text{act}} \Delta, \end{aligned} \tag{18}$$

where $\Delta = [\delta_1, \dot{\delta}_1, \dots, \delta_4, \dot{\delta}_4]^T$, $B_{\text{act}} = B_{8 \times 4} \mathbf{T}$ and $y_{\text{act}} = [\delta_1, \delta_2, \delta_3, \delta_4]$ is the output of the actuator. The set of equations on the right hand side describes a 21st-order rigid body plus slosh system where the terms in $B_{21 \times 4}^*$ are terms in $A_{21 \times 8}^*$ corresponding to $\delta_1, \delta_2, \delta_3$ and δ_4 . We re-write this system as

$$\begin{aligned} K_0 \dot{x}_0 &= A_0 x_0 + B_0 y_{\text{act}} \\ y &= C_0 x_0, \end{aligned} \tag{19}$$

where x_0 is a state vector consisting of the 5 rigid body and 16 slosh state variables. Since K_0 is invertible we have

$$\begin{aligned} \dot{x}_0 &= A_{01} x_0 + B_{01} y_{\text{act}} \\ y &= C_0 x_0, \end{aligned} \tag{20}$$

where $A_{01} = K_0^{-1}A_0$ and $B_{01} = K_0^{-1}B_0$. The system (20) is a 4 input and 4 output system. For the purpose of controller design we neglect the actuator dynamics and hence (14), (18) and (20) give a 2 input 4 output system given by

$$\dot{x}_0 = A_{01}x_0 + B'_{01}u' \quad y = C_0x_0, \quad (21)$$

where $B'_{01} = B_{01}\mathbf{T}$. The system (21) is analysed and found to be controllable and observable though unstable.

4. LQG controller synthesis

We now carry out LQG synthesis (Athans 1971) for the LV system. The expression for the LQG compensator, a dynamic output feedback compensator made up of regulator and filter, is given by

$$u(s) = -K_c(sI - A + BK_c + K_fC)^{-1}K_f y(s),$$

where K_c is regulator gain matrix and K_f is Kalman filter gain matrix. The K_c is calculated such that it minimizes the performance criterion

$$J(\mathbf{x}, t_0, T, \mathbf{u}(\cdot)) = \int_{t_0}^T [\mathbf{x}^T Q \mathbf{x} + \mathbf{u}^T R \mathbf{u}] dt, \quad (22)$$

and K_f is such that it gives optimal least-squares estimate for the given random process noise and observation noise co-variances, $W \geq 0$ and $V > 0$ respectively. These conditions lead to the Riccati equations, solving which the gain matrices are obtained (Athans 1971). In this work, all such computations were performed on MATLAB. However, the choice of the weighting matrices $Q \geq 0$, $R > 0$, W , and V is somewhat arbitrary and is obtained by some experimentation.

Here, two LQG controllers are presented for the system discussed in § 4. The first design yields a 21st-order controller and the second one a 5th-order. Since the actuator dynamics have not been incorporated at the control algorithm design stage, these controllers should have sufficient robustness. Further, requirements on maximum allowed actuator deflection $\pm 6^\circ$ must not be violated.

4.1 Design 1

Initially, the weighting matrices are selected as unity matrices of appropriate size multiplied by a scalar, and by varying the value of the scalar some iterations are done. To obtain a better controller it is essential to vary individual entries in the weighting matrices. Since working with a 21st-order weighting matrices is difficult, smaller weighting matrices are designed for a 5th-order rigid body system by neglecting the slosh dynamics. The smaller weightings are selected such that the closed loop with the rigid body dynamics alone exhibits a good response. Then these smaller weighting matrices are inserted into the larger unity matrices of appropriate size. The weighting matrices hence obtained are

$$\mathbf{Q} = \left[\begin{array}{ccc|c} 100 & 8 & 2 & \\ 8 & 1 & 0.5 & \emptyset \\ 2 & 0.5 & 1 & \\ \hline & \emptyset & & [\mathbf{I}]_{18} \end{array} \right], \quad \mathbf{W} = 4.5[\mathbf{I}]_{21} \quad \mathbf{R} = [\mathbf{I}]_2, \quad \text{and} \quad \mathbf{V} = [\mathbf{I}]_4.$$

The controller thus obtained has poles at

$$\begin{array}{cccc} -90.1860 & -67.9762 & -3.0676 \pm 3.2380i & -0.0003 \\ -2.6270 & -3.2668 & -1.7124 \pm 1.9813i & -0.1201 \pm 6.9445i \\ -0.0221 \pm 6.8952i & -0.0245 \pm 7.2868i & -0.0302 \pm 7.0240i & -0.0259 \pm 7.1571i \\ -0.0788 \pm 7.1460i & & & \end{array}$$

It places the closed loop poles at

$$\begin{array}{cccc} -76.9727 \pm 78.5298i & -76.9738 \pm 78.5301i & -86.1156 & -55.0164 \pm 55.2954i \\ -54.4865 \pm 53.6319i & -64.7763 & -18.0727 \pm 16.5830i & -19.3835 \pm 14.0794i \\ -17.5929 \pm 17.9484i & -17.5929 \pm 17.9484i & -4.5916 & -2.6400 \\ -2.4772 \pm 1.1699i & -0.6497 \pm 1.5284i & -1.4352 \pm 1.6471i & -0.0274 \\ -0.4804 & -1.1468 & -0.9021 & -0.0823 \pm 7.7049i \\ -0.0596 \pm 7.4227i & -0.0243 \pm 7.2866i & -0.0222 \pm 7.2840i & -0.1160 \pm 6.9500i \\ -0.0220 \pm 6.8953i & -0.0207 \pm 6.8928i & -0.0214 \pm 6.9262i & -0.0773 \pm 7.1459i \\ -0.0299 \pm 7.0241i & -0.0258 \pm 7.1568i & -0.0211 \pm 7.0241i & -0.0259 \pm 7.1384i \\ -0.0215 \pm 7.1544i & & & \end{array}$$

4.2 Design 2

Design 1 gives a 21st-order controller which may be difficult to implement and will increase the closed-loop order significantly. Hence a controller of smaller order is designed. For this purpose the 5th-order rigid body system is used.

For selecting the weighting matrices, the rigid body system is further divided into pitch and roll systems. Since the system is a 2 input 4 output one, out of two singular value plots one belongs to the pitch and the other to the roll. The objective is to keep these singular value plots for the closed loop system as close to each other in the bandwidth of operation/interest. The smaller order weighting matrices are then augmented to get a 5th-order weighting matrix which is further manipulated to get a better performance. The weighting matrices thus obtained are

$$\begin{aligned} \mathbf{Q} &= \text{diag}\{20, 0.01, 0.1, 1, 1\}, \quad \mathbf{R} = 10[\mathbf{I}]_2, \\ \mathbf{W} &= \text{diag}\{100, 500, 0.1, 150, 150\}, \quad \mathbf{V} = \text{diag}\{10, 10, 1, 1\}. \end{aligned}$$

The controller poles are at -3.4018 , -0.0252 , -8.8524 , -15.5837 , -12.8088 and the closed-loop poles are located at

$$\begin{array}{cccc} -76.9718 \pm 78.5275i & -76.9711 \pm 78.5297i & -55.1398 \pm 55.9984i & -55.4722 \pm 55.7587i \\ -18.1949 \pm 18.6189i & -19.9718 \pm 19.8129i & -12.6460 & -5.5094 \\ -4.3452 \pm 1.8577i & -3.2949 & -0.9300 \pm 0.6270i & -0.0272 \\ -0.0682 & -1.0889 & -0.1178 \pm 7.7798i & -0.0413 \pm 7.4630i \\ -0.0208 \pm 6.8931i & -0.0215 \pm 6.9278i & -0.0220 \pm 7.2840i & -0.0212 \pm 7.0245i \\ -0.0215 \pm 7.1548i & -0.0239 \pm 7.1396i & -17.5929 \pm 17.9484i & -17.5929 \pm 17.9484i \end{array}$$

5. Simulation results

In this section, we demonstrate the effectiveness of the controller by performing simulations of the closed-loop system shown in figure 4. The controller performance is validated with the full 29th-order system in the closed-loop. The closed-loop system is the system between the

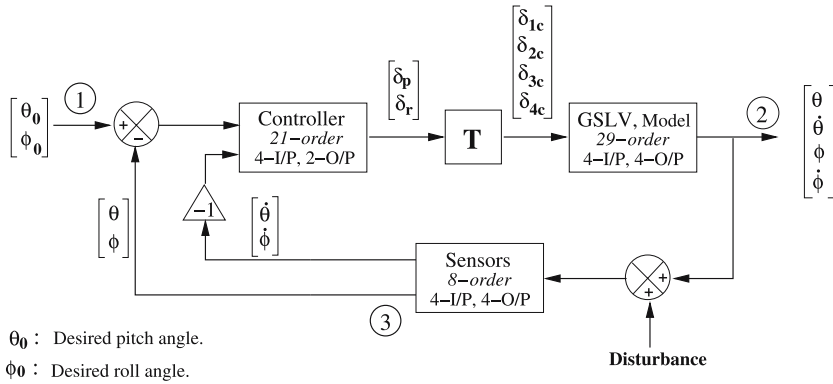


Figure 4. Closed-loop step response.

points 1 and 2, and the output signals plotted are taken from point 3. A step input is applied separately in the pitch and roll channel. The step response, actuator deflection and deflection of the slosh pendulums are plotted. The step is 1° (0.017 rad) in magnitude and applied at time $t = 0$ sec.

The step response with controller 1 is better for the pitch channel, while the response of the roll channel is better with controller 2 (figure 5). Though the pitch response with controller 1 shows a peak overshoot it reaches steady state faster, while in the roll channel the step response of controller 2 is faster. In all the cases the actuator deflections are well within the allowable limits, see figure 6. Figure 7 shows sloshing excited due to the application of the step input in the pitch channel. The slosh is suppressed well with controller 1, but in the case of controller 2, the oscillations are sustained for a long period of time indicative of the fact that at the design stage the slosh dynamics was neglected. Figure 8 shows the Nyquist plots for the pitch and roll channel. The pitch channel closed-loop is the transfer function from δ_p to θ and for roll channel it is the transfer function from δ_r to ϕ . The plot depicts that the gain and phase margins are larger for the system with controller 2. The Bode plots for the same system are shown in figure 9. The sharp spikes in the magnitude plots show the effect of slosh near 7 rad/sec and the effect of actuator near 25 rad/sec. The phase plot shows the effect of the actuator dynamics on the system phase.

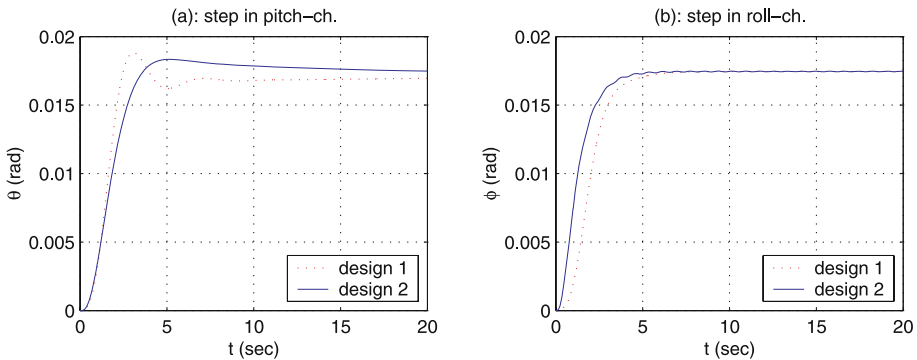


Figure 5. Closed-loop step response.

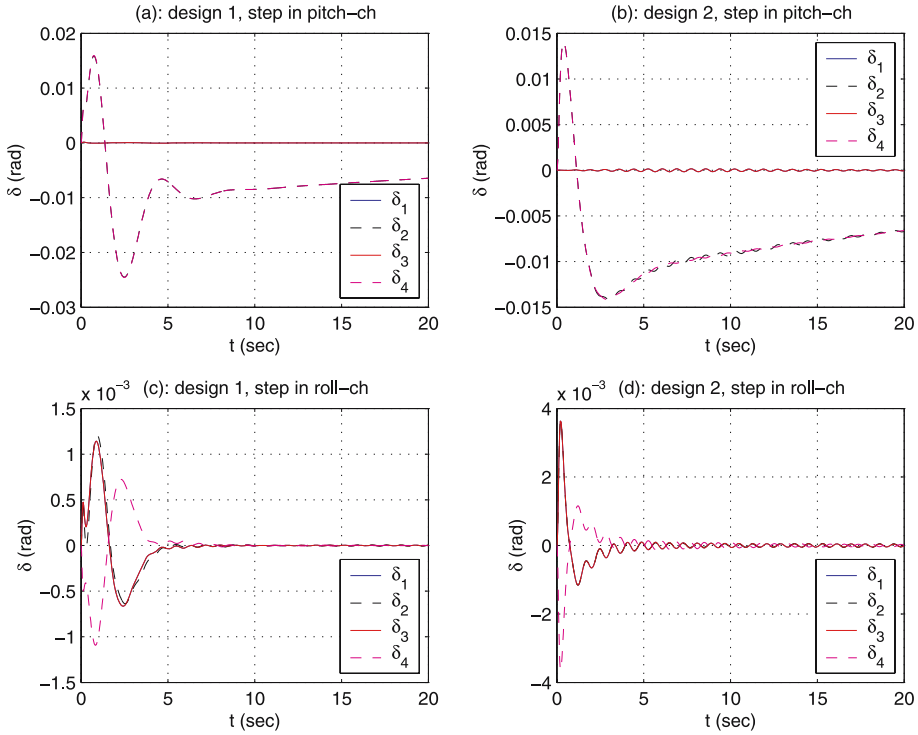


Figure 6. Actuator deflection corresponding to response plotted in figure 5.

6. Conclusion

In this paper, we have synthesized a LQG controller for a 29th-order perturbation model of a LV. A system that is appropriate for LQG design is obtained from the given system by separating the actuator dynamics from the slosh and rigid body dynamics. If a large system comprises of a main system and many smaller systems coupled to it, then with some assumptions the smaller systems can be separated from the main system. If a controller is designed for the

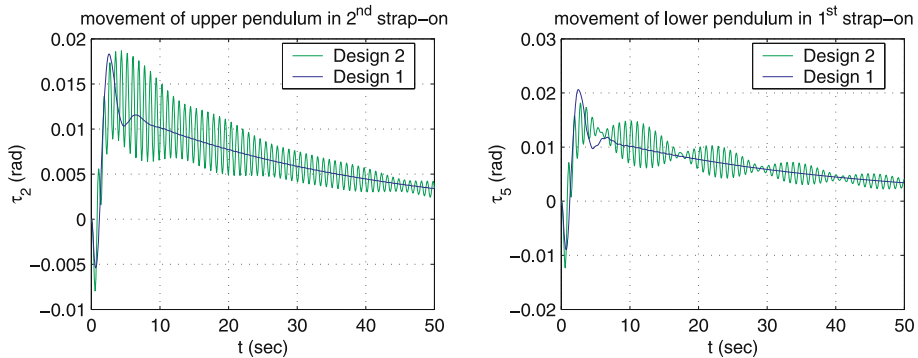


Figure 7. Fuel slosh in response to step in pitch channel.

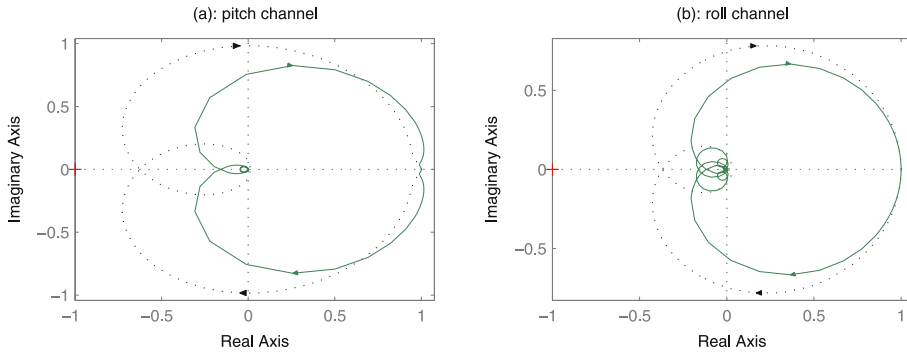


Figure 8. Nyquist plots, (...) design 1 and (—) design 2.

main system with significant robustness then the original large system can be successfully controlled with the same controller. Here two controllers are presented, one is 21st-order and the other is 5th-order. The smaller order controller gives better performance and is more robust than the other controller. The weights can be further manipulated to get better performance and robustness.

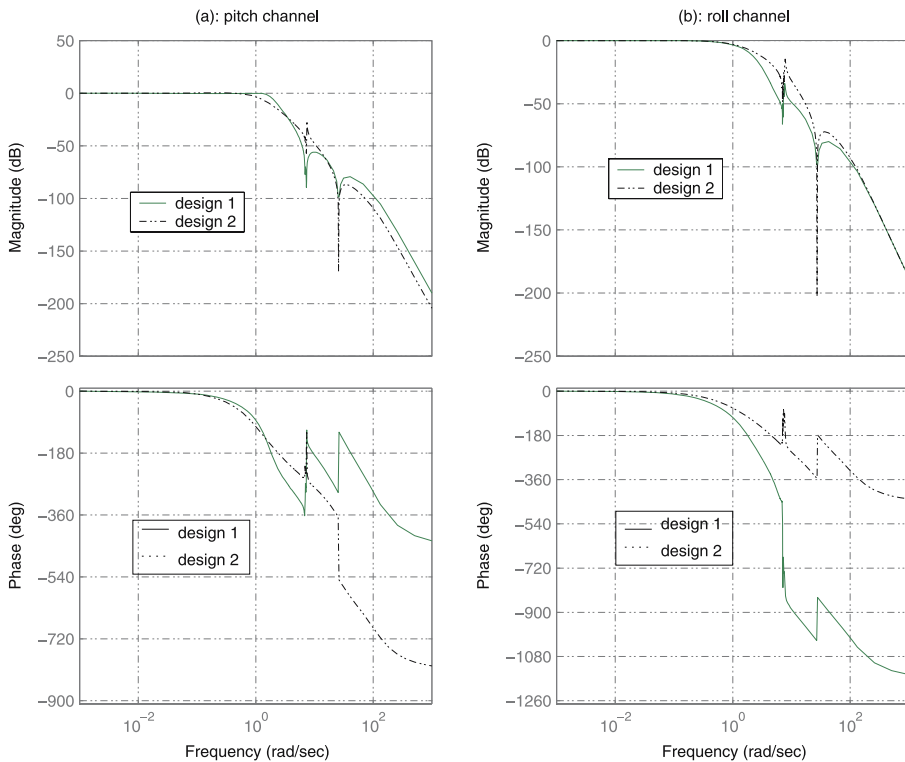


Figure 9. Bode plot.

7. List of symbols

θ	perturbation angle in pitch
I_R	engine inertia
m_R	mass of the engine
l_R	distance between engine CG and gimbal point
l_c	control location
δ_i	actuator deflection
I_{yy}	moment of inertia - pitch
L_α	aerodynamic force
l_α	aerodynamic moment arm
α	angle of attack
\dot{U}_0	forward acceleration
m_{pi}	mass of i^{th} pendulum (I mode)
l_{pi}	hinge point of i^{th} pendulum (I mode)
τ_{pi}	slosh pendulum angle
ζ_{pi}	slosh damping
ω_{pi}	slosh frequency, same for upper and lower pendulums
μ_{pi}	slosh pendulum velocity
T_c	control thrust
m_0	reduced mass of vehicle
U_0	forward velocity
ϕ	perturbation angle - roll
I_{xx}	moment of inertia - roll
l_ϕ^R	roll moment arm lop
l_ϕ^{OP}	out of plane roll moment arm
ζ_a	actuator damping
ω_a	actuator natural frequency

References

- Abramson H 1966 *The dynamic behaviour of liquids in moving containers*, NASA SP-106. National Aeronautics and Space Administration
- Athans M 1971 'The role and use of the LQG controller in control system design,' *IEEE Trans. on Automatic Control*, 21:
- Dhabale A, Banavar R N, Dhekane M V LQG controller designs from reduced order models for a launch vehicle, In *Proceedings of the 2005 IFAC World Congress*
- Dodge F T and Garza L R 1967 'Experimental and theoretical studies of liquid sloshing at simulated low gravity,' *J. Appl. Mech., Transaction of ASME*, 555–562
- Greensite A 1972 *Control theory: Analysis and design of space vehicle flight control systems*. Spartan Books
- Reyhanoglu M, Cho S, McClamroch N H 1999 Feedback control for planar maneuvers of an aerospace vehicle with an unactuated internal degree of freedom, In *Proceedings of the American Control Conference*, (San Diego, CA), 3432–3436
- Reyhanoglu M, Cho S, McClamroch N H 2000 Discontinuous feedback control of a special class of underactuated mechanical systems, *Int. J. Robust and Nonlinear Control*, 24: 265–281